Research Article | Vol. 26, No. 10 | 14 May 2018 | OPTICS EXPRESS 12790
Optics EXPRESS

Dual-wavelength, mode-locked erbium-doped fiber laser employing a graphene/polymethyl-methacrylate saturable absorber

K. Y. Lau,[1] M. H. Abu Bakar,[1] F. D. Muhammad,[2] A. A. Latif,[2] M. F. Omar,[3] Z. Yusoff,[4] and M. A. Mahdi[1,*]

[1]*Wireless and Photonics Networks Research Centre, Faculty of Engineering, Universiti Putra Malaysia, 43400 UPM Serdang, Selangor, Malaysia*
[2]*Department of Physics, Faculty of Science, Universiti Putra Malaysia, 43400 UPM Serdang, Selangor, Malaysia*
[3]*Physics Department, Faculty of Science, Universiti Teknologi Malaysia, 81310 Skudai, Johor, Malaysia*
[4]*Fiber Optic Research Centre, Faculty of Engineering, Multimedia University, 63100 Cyberjaya, Selangor, Malaysia*
[*]*mam@upm.edu.my*

Abstract: Mode-locked fiber laser incorporating a saturable absorber is an attractive configuration due to its stability and simple structure. In this work, we demonstrate a dual-wavelength passively mode-locked erbium-doped fiber laser employing a graphene/polymethyl-methacrylate saturable absorber. A laser resonator is developed based on dual cavity architecture with unidirectional signal oscillation, which is connected by a fiber branch sharing a common gain medium and saturable absorber. Dual wavelength mode-locked fiber lasers are observed at approximately 1530 and 1560 nm with 22.6 mW pump power threshold. Soliton pulse circulates in the laser cavity with pulse duration of 900 and 940 fs at shorter and longer wavelengths, respectively. This work presents a viable option in developing a low threshold mode-locked laser source with closely spaced dual wavelength femtosecond pulses in the C-band wavelength region.

OCIS codes: (140.4050) Mode-locked lasers; (320.7110) Ultrafast nonlinear optics.

References and links

1. Z. Luo, Y. Huang, J. Wang, H. Cheng, Z. Cai, and C. Ye, "Multiwavelength dissipative-soliton generation in Yb-fiber laser using graphene-deposited fiber-taper," IEEE Photonics Technol. Lett. **24**(17), 1539–1542 (2012).
2. D. Pudo, L. R. Chen, D. Giannone, L. Zhang, and I. Bennion, "Actively mode-locked tunable dual-wavelength erbium-doped fiber laser," IEEE Photonics Technol. Lett. **14**(2), 143–145 (2002).
3. Y.-G. Han, T. V. A. Tran, and S. B. Lee, "Wavelength-spacing tunable multiwavelength erbium-doped fiber laser based on four-wave mixing of dispersion-shifted fiber," Opt. Lett. **31**(6), 697–699 (2006).
4. M. H. Al-Mansoori, M. K. Abd-Rahman, F. R. Mahamd Adikan, and M. A. Mahdi, "Widely tunable linear cavity multiwavelength Brillouin-Erbium fiber lasers," Opt. Express **13**(9), 3471–3476 (2005).
5. J. Yao, J. Yao, Y. Wang, S. C. Tjin, Y. Zhou, Y. L. Lam, J. Liu, and C. Liu, "Active mode locking of tunable multi-wavelength fiber ring laser," Opt. Commun. **191**(3), 341–345 (2001).
6. J. Yao, J. Yao, and Z. Deng, "Multiwavelength actively mode-locked fiber ring laser with suppressed homogeneous line broadening and reduced supermode noise," Opt. Express **12**(19), 4529–4534 (2004).
7. A. Martinez and Z. Sun, "Nanotube and graphene saturable absorbers for fibre lasers," Nat. Photonics **7**(11), 842–845 (2013).
8. S. Yamashita, Y. Inoue, S. Maruyama, Y. Murakami, H. Yaguchi, M. Jablonski, and S. Y. Set, "Saturable absorbers incorporating carbon nanotubes directly synthesized onto substrates and fibers and their application to mode-locked fiber lasers," Opt. Lett. **29**(14), 1581–1583 (2004).
9. Q. Bao, H. Zhang, J.-X. Yang, S. Wang, D. Y. Tang, R. Jose, S. Ramakrishna, C. T. Lim, and K. P. Loh, "Graphene-polymer nanofiber membrane for ultrafast photonics," Adv. Funct. Mater. **20**(5), 782–791 (2010).
10. Z. Sun, T. Hasan, F. Torrisi, D. Popa, G. Privitera, F. Wang, F. Bonaccorso, D. M. Basko, and A. C. Ferrari, "Graphene mode-locked ultrafast laser," ACS Nano **4**(2), 803–810 (2010).
11. X. He, X. Zhang, H. Zhang, and M. Xu, "Graphene covered on microfiber exhibiting polarization and polarization-dependent saturable absorption," IEEE J. Sel. Top. Quantum Electron. **20**(1), 55–61 (2014).

#325602 https://doi.org/10.1364/OE.26.012790
Journal © 2018 Received 8 Mar 2018; revised 18 Apr 2018; accepted 19 Apr 2018; published 3 May 2018

Optics EXPRESS

12. Q. Sheng, M. Feng, W. Xin, T. Han, Y. Liu, Z. Liu, and J. Tian, "Actively manipulation of operation states in passively pulsed fiber lasers by using graphene saturable absorber on microfiber," Opt. Express **21**(12), 14859–14866 (2013).
13. W. Xin, Z. B. Liu, Q. W. Sheng, M. Feng, L. G. Huang, P. Wang, W. S. Jiang, F. Xing, Y. G. Liu, and J. G. Tian, "Flexible graphene saturable absorber on two-layer structure for tunable mode-locked soliton fiber laser," Opt. Express **22**(9), 10239–10247 (2014).
14. J. M. Dawlaty, S. Shivaraman, M. Chandrashekhar, F. Rana, and M. G. Spencer, "Measurement of ultrafast carrier dynamics in epitaxial graphene," Appl. Phys. Lett. **92**(4), 042116 (2008).
15. Z. Q. Luo, J. Z. Wang, M. Zhou, H. Y. Xu, Z. P. Cai, and C. C. Ye, "Multiwavelength mode-locked erbium-doped fiber laser based on the interaction of graphene and fiber-taper evanescent field," Laser Phys. Lett. **9**(3), 229–233 (2012).
16. N. Zhao, M. Liu, H. Liu, X.-W. Zheng, Q.-Y. Ning, A.-P. Luo, Z.-C. Luo, and W.-C. Xu, "Dual-wavelength rectangular pulse Yb-doped fiber laser using a microfiber-based graphene saturable absorber," Opt. Express **22**(9), 10906–10913 (2014).
17. J. Sotor, G. Sobon, J. Tarka, I. Pasternak, A. Krajewska, W. Strupinski, and K. M. Abramski, "Passive synchronization of erbium and thulium doped fiber mode-locked lasers enhanced by common graphene saturable absorber," Opt. Express **22**(5), 5536–5543 (2014).
18. H. R. Yang, "Switchable dual-wavelength fiber laser mode-locked by monolayer graphene on D-shaped fiber," J. Mod. Opt. **62**(17), 1363–1367 (2015).
19. F. D. Souza and K. M. Kadish, *Handbook of Carbon Nano Materials* (World Scientific, 2010), Chap. 5.
20. A. Kaniyoor and S. Ramaprabhu, "A Raman spectroscopic investigation of graphite oxide derived graphene," AIP Adv. **2**(3), 032183 (2012).
21. H. J. Kim, S.-M. Lee, Y.-S. Oh, Y.-H. Yang, Y. S. Lim, D. H. Yoon, C. Lee, J.-Y. Kim, and R. S. Ruoff, "Unoxidized graphene/alumina nanocomposite: Fracture- and wear-resistance effects of graphene on alumina matrix," Sci. Rep. **4**(1), 5176 (2014).
22. S. Stankovich, D. A. Dikin, R. D. Piner, K. A. Kohlhaas, A. Kleinhammes, Y. Jia, Y. Wu, S. B. T. Nguyen, and R. S. Ruoff, "Synthesis of graphene-based nanosheets via chemical reduction of exfoliated graphite oxide," Carbon **45**(7), 1558–1565 (2007).
23. M. M. Lucchese, F. Stavale, E. H. Martins Ferreira, C. Vilani, M. V. O. Moutinho, R. B. Capaz, C. A. Achete, and A. Jorio, "Quantifying ion-induced defects and Raman relaxation length in graphene," Carbon **48**(5), 1592–1597 (2010).
24. D. L. Mafra, G. Samsonidze, L. M. Malard, D. C. Elias, J. C. Brant, F. Plentz, E. S. Alves, and M. A. Pimenta, "Determination of LA and TO photon dispersion relations of graphene near the Dirac point by double resonance Raman scattering," Phys. Rev. B **76**(23), 233407 (2007).
25. K. J. Thomas, M. Sheeba, V. P. N. Nampoori, C. P. G. Vallahan, and P. Radhakrishnan, "Raman spectra of polymethyl methacrylate optical fibres excited by a 532 nm diode pumped solid state laser," J. Opt. A, Pure Appl. Opt. **10**(5), 055303 (2008).
26. T. S. Kavetskyy and A. L. Stepanov, *Radiation Effects in Materials* (InTech, 2016), Chap. 11.
27. P. Yan, A. Liu, Y. Chen, J. Wang, S. Ruan, H. Chen, and J. Ding, "Passively mode-locked fiber laser by a cell-type WS_2 nanosheets saturable absorber," Sci. Rep. **5**(1), 12587 (2015).
28. A. Martinez, K. Fuse, B. Xu, and S. Yamashita, "Optical deposition of graphene and carbon nanotubes in a fiber ferrule for passive mode-locked lasing," Opt. Express **18**(22), 23054–23061 (2010).
29. J. Sotor, G. Sobon, K. Grodecki, and K. M. Abramski, "Mode-locked erbium-doped fiber laser based on evanescent field interaction with Sb_2Te_3 topological insulator," Appl. Phys. Lett. **104**(25), 251112 (2014).
30. H. Zhang, D. Tang, R. J. Knize, L. Zhao, Q. Bao, and K. P. Loh, "Graphene mode locked, wavelength-tunable, dissipative soliton fiber laser," Appl. Phys. Lett. **96**(11), 111112 (2010).
31. G. Sobon, J. Sotor, and K. M. Abramski, "All-polarization maintaining femtosecond Er-doped fiber laser mode-locked by graphene saturable absorber," Laser Phys. Lett. **9**(8), 581–586 (2012).
32. Y. Chen, M. Wu, P. Tang, S. Chen, J. Du, G. Jiang, Y. Li, C. Zhao, H. Zhang, and S. Wen, "The formation of various multi-soliton patterns and noise-like pulse in a fiber laser passively mode-locked by a topological insulator," Laser Phys. Lett. **11**(5), 055101 (2014).
33. Y. Wang, S.-U. Alam, E. D. Obraztsova, A. S. Pozharov, S. Y. Set, and S. Yamashita, "Generation of stretched pulses and dissipative solitons at 2 μm from an all-fiber mode-locked laser using carbon nanotube saturable absorbers," Opt. Lett. **41**(16), 3864–3867 (2016).

1. Introduction

Compact optical sources producing multiple wavelengths are extremely crucial in many applications such as photonics component characterization, optical communications, fiber optic sensing, and microwave/terahertz photonics [1]. A big challenge in generating stable multiwavelength in erbium-doped fiber laser (EDFL) is the mode competition in the gain medium at room temperature, making it difficult to obtain simultaneous multiwavelength operation with closely spaced lines [2]. Therefore, various approaches have been taken to

Optics EXPRESS

realize multiwavelength oscillation such as by introducing nonlinear effect to the fiber laser with four-wave mixing [3] and stimulated Brillouin scattering [4].

Apart from continuous wave multiwavelength fiber lasers, actively mode-locked multiwavelength lasing has been proposed by Yao et al. using a single sampled fiber Bragg grating [5] as well as a biased semiconductor optical amplifier [6]. Although multiwavelength actively mode-locked fiber laser has advantages such as high repetition rate, the incorporation of bulky device in the cavity introduces high insertion loss and increases the system complexity. Therefore, all-fiber passively mode-locked multiwavelength fiber laser is more desirable. In particular, passively mode-locked multiwavelength fiber laser using saturable absorber (SA) allows for more robust, compact and efficient fiber laser systems to be realized.

SAs can take many forms but of late, the allotropes of carbon such as graphene and carbon nanotubes (CNTs) have proven themselves to be very capable as SAs for mode-locked lasers with multiple wavelengths operation [7, 8]. Graphene, a single layer of carbon atom [9–11] has seen substantial deployment as SA due to its remarkable properties such as ultra-broadband absorption and gapless linear dispersion of massless Dirac like particles [12, 13]. Under high excitation intensities, the concentration of photo-generated carriers is increased, surpassing the intrinsic hole and electron carrier densities of 8 x 10^{10} cm^{-2} [14]. This condition forces the filling of the state near the edges of lower and upper Dirac-cones. The supplementary absorption is halted when every single state above the edges of upper Dirac-cone is occupied with photons during saturable absorption. This imparts light transparency as a function of photon energies exactly at the band edges. The saturable absorption due to the Pauli blocking effect in graphene hybrid materials combined with ultrafast carrier dynamics provides strong optical nonlinearity with fast response time for mode-locking operation.

The utilization of graphene for obtaining a multiwavelength passively mode-locked EDFL with closed wavelength spacing based on fiber-taper evanescence interaction has been demonstrated in [15]. Moreover, Zhao et al. [16] had demonstrated dual-wavelength passively mode-locked ytterbium-doped fiber laser at approximately 1 μm operating wavelength. Narrow spectral bandwidths in both works [15, 16] led to pulse duration measurement in picosecond range. Apart from that, Sotor et al. [17] has demonstrated a passively synchronized erbium and thulium-doped fiber mode-locked lasers enhanced by graphene SA, with secant hyperbolic ($sech^2$) fitted pulse duration of 0.915 and 1.57 ps, respectively. However, the dual-wavelength mode-locked laser emitted by this technique has an extremely large wavelength difference, making it less attractive for certain applications that require closely spaced lines. Furthermore, this design requires two different gain media pumped by two different laser diodes and significant control of delay line at erbium loop, thus increasing the design complexity. A dual-wavelength mode-locked EDFL is thereafter presented at around 1530 and 1560 nm simultaneously by controlling the intra-cavity loss using different polarization controller status, but with the achievement of only picosecond pulses [18].

In this work, we demonstrate simpler laser configurations that produce closely spaced dual-wavelength pulses with passive mode-locking regime enabled by graphene/polymethyl-methacrylate (PMMA) saturable absorber (GPSA). The configuration is based on a separate cavity loop for each different lasing wavelength connected by a fiber branch with a common gain medium and SA. Such design is able to generate simultaneous optical solitons with pulse duration of 900 and 940 fs centered at approximately 1530 and 1560 nm, respectively, which is a feat that has yet to be achieved by other existing graphene approaches [15–18]. This mode-locked laser shows its practicality in numerous applications, such as laser marking, signal processing and supercontinuum source generation by employing high nonlinear medium.

2. Fabrication and material characterization of GPSA

The graphene/PMMA-thin film (GPTF) consists of a tri-layer structure in which the graphene is sandwiched between PMMA and polymer substrate. The thickness of single graphene layer

Optics EXPRESS

and PMMA layer is 0.34 and 500 nm, respectively. Figure 1(a) shows the microscopic image of GPTF taken at the edge of this film using an Olympus LEXT OLS 4100 Laser Scanning Digital Microscope. This microscope can identify a measuring position and perform accurate surface roughness measurement of a micro area at 10 nm resolution regardless of surface texture condition. There are two distinctive color regions observed through microscopic image in Fig. 1(a); rainbow-like and greyish. The rainbow-like region denotes the GPTF whilst the greyish region is the polymer substrate with uneven surface roughness. On the other hand, the height map of the sample as a function of distance from the microscope lens as depicted in Fig. 1(b).

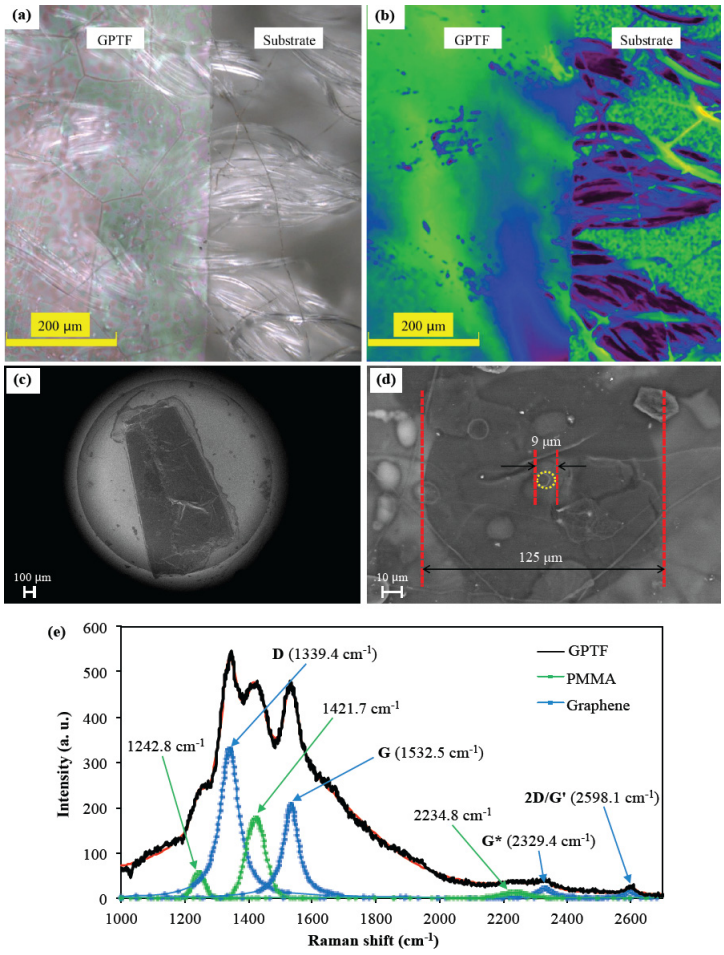

Fig. 1. (a) Microscopic image and (b) height map of GPTF on polymer substrate, FESEM images of GPTF on a fiber ferrule with magnification sized of (c) 80x and (d) 1500x, and (e) Raman spectrum of GPTF at the fiber core region.

The green color perceives areas which are closer to the microscope lens as compared to the purple color. The presence of blue and purple colors within this GPTF region is due to the uneven thickness of the underneath polymer substrate, particularly the "fiber-like" texture regions. In order to separate the GPTF from the polymer substrate, several water droplets are dropped at the edge of the GPTF to detach the GPTF from the polymer substrate. The detached GPTF is then carefully picked up and immersed in a water bath. After that, the GPTF is transferred onto a piece of filter paper. The GPTF on the filter paper is then cut into a dimension of approximately 2 mm x 2 mm and placed onto a single-mode fiber ferrule

Optics EXPRESS

using tweezers with the PMMA layer facing the ferrule surface. The filter paper is then peeled off and the GPTF is left to dry on the fiber ferrule for 10 minute.

The morphology of GPTF on the fiber ferrule is then examined using Zeiss Crossbeam 340 field emission scanning electron microscope (FESEM) system in variable pressure mode as shown in Fig. 1(c) and 1(d). The variable pressure mode is activated to avoid charging effect on the optical fiber. Therefore, no conductive coating is required during the analysis. Figure 1(c) shows the fiber ferrule region observed with a magnification size of 80x. From the analysis, the GPTF covers the entire core region. Wrinkles observed on the GPTF could be due to dehydration of the material layer. A closer look at the fiber cladding and core regions are achieved with a magnification size of 1500x as depicted in Fig. 1(d). In order to have a better image contrast relative to element atomic number, a back-scattered electron detector is utilized. The fiber cladding is annotated with the circle measured at 125 μm diameter. Additionally, the circle with smaller diameter at 9 μm portrays the boundary of fiber core region. Several bright ring shape spots are observed in Fig. 1(d) that represent contaminated areas formed due to the long electron exposure time during image focusing process.

The GPTF on fiber ferrule is then examined using micro-Raman spectroscopy (Horiba JY, Xplora Plus, France) with a 100x objective (laser spot, ~1 μm^2) and 1200 mm^{-1} grating. The laser excitation wavelength is 785 nm (~1.57 eV). The acquisition time used for measurement is 10 s with 10 accumulations. Calibration is conducted by checking the Si band at 520.7 cm^{-1} and peaks are fitted using the Origin software. This excitation wavelength is used due to the presence of fluorescence around 550 nm regions. For a detailed analysis, Fig. 1(e) shows the Raman spectrum of GPTF and its fitted peaks of graphene and PMMA. The background has been subtracted before fitting is carried on. The spectrum is fitted using Lorentzian and Gaussian approximation for graphene and PMMA respectively. Graphene is fitted using Lorentzian curve with full width half maximum (FWHM) range from 50 to 55 cm^{-1}. The peaks observed at Raman shift of 1242.80 and 1421.70 cm^{-1} indicate organic chemical bonding of PMMA as described in [26]. In addition, the typical D, G, G* and 2D(G') bands of graphene are obtained at 1339.40, 1532.50, 2329.40, and 2598.10 cm^{-1}, respectively. The intensity of 2D band to G band (I_{2D}/I_G) of less than two concludes the multiple-layered state of graphene on the fiber core [19]. The intensity of D band to G band (I_D/I_G) of more than 1.0 reveals the presence of multiple graphene layers possibly due to creases introduced during the deposition process [20]. It could also be due to the formation of graphene oxide defect [21, 22] after long exposure to high-energy electron beam in low vacuum mode during FESEM analysis [23]. On the other hand, 2D (G') band and G* band shows red-shifted and blue-shifted effects, respectively owing to the lower energy laser excitation used for Raman experiment as explained in [24]. A small hump at 2234.8 cm^{-1} is attributed to the interaction between PMMA and graphene layer, as it has not been observed in pure PMMA [25, 26].

3. Optical characterization of GPSA

The nonlinear saturable absorption properties of the GPSA is characterized by a pulsed laser source (PLS) with pulse repetition rate and pulse duration of 250 MHz and 120 fs, respectively at 1550 nm central wavelength [27]. The setup for this measurement is shown in Fig. 2(a). A variable optical attenuator (VOA) is used to tune the pump power of the pulsed laser source. An isolator (ISO) is placed in between the VOA and a 3-dB coupler to prevent the signal from returning to the pulsed laser source. Two equal portions of the output signals [Optical Path 1 (OP1) and Optical Path 2(OP2)] are generated by splitting the input signal through the 3-dB coupler. The GPSA is fusion spliced within OP1 for reference power measurement. On the other hand, OP2 is set up for power-dependent transmission measurement. The output power of both OP1 and OP2 are simultaneously measured using optical power meters (OPM-1 and OPM-2) respectively. The corresponding nonlinear saturable absorption curve of the GPSA as a function of peak intensity is shown in Fig. 2(b). From this curve, the modulation depth (MD) can be determined, giving a value of 6% which

Optics EXPRESS

is sufficient to initiate mode-locking operation [28]. In addition, the saturation intensity (I_{sat}), which is the required optical intensity to achieve the semi-absorption state for an unbleached SA [29] can also be estimated from the nonlinear saturation transmittance curve. Based on the figure, the measured I_{sat} of the GPSA is 3.4 MW/cm^2.

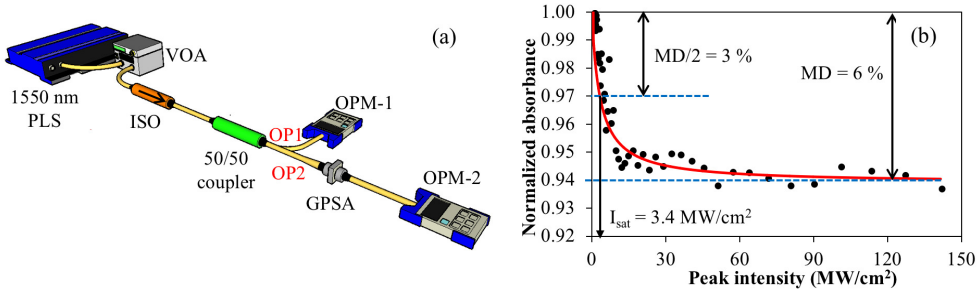

Fig. 2. (a) Nonlinear saturable absorption measurement setup and (b) measurement of GPSA.

4. Dual-wavelength mode-locked fiber laser

The experimental setup of the dual-wavelength passively mode-locked EDFL with unidirectional signal propagation in the main loop is depicted in Fig. 3. A section of 4.5 m erbium-doped fiber (EDF) with signal absorption coefficient of 3.5 dB/m at 1530 nm is utilized as the active gain medium and pumped by a 980 nm laser diode (LD) via a 980/1550 nm wavelength division multiplexer (WDM). The GPSA is placed at the output port of the EDF to generate the mode-locked laser. The polarization state of the laser cavity is tuned by a polarization controller (PC) that is connected at the output of the GPSA to control cavity birefringence effects. A red/blue wavelength division multiplexer (R/B WDM-1) is employed to split the input signal into the shorter wavelength, λ(-) from 1530 to 1543 nm and longer wavelength, λ(+) from 1547 to 1561 nm. The portion of λ(-) is guided to an optical coupler (OC-1), while the other portion of λ(+) is guided to another optical coupler (OC-2) to extract 30% of each signal for further analysis (OP-1 and OP-2). The remaining signals of both λ(-) and λ(+) portions are then channeled through the 70% port of OC-1 and OC-2 respectively and are recombined at R/B WDM 2. An isolator (ISO) is placed in between the R/B WDM-2 and the 1550 nm port of the WDM to force unidirectional signal propagation in the common branch of the laser resonator.

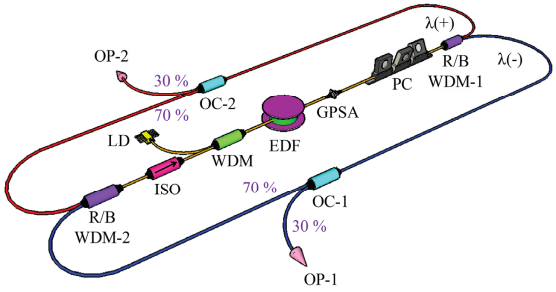

Fig. 3. Experimental setup for dual-wavelength mode-locked fiber laser, denoted as MLFL-U.

To measure the net dispersion of the entire laser cavity, the group velocity dispersion (GVD) of each type of optical fiber is calculated. These optical fibers include Corning SMF-28, Corning Hi-1060 SMF, and Lucent Technologies HP980 EDF. The dispersion coefficients, β_2 of these optical fibers at C-band are approximately –22, –7 and 23 ps^2/km, respectively. The net GVD of each type of optical fibers is calculated. The total GVD of the λ(-) and λ(+) optical paths for MLFL-U is estimated to be –0.3215 and –0.2797 ps^2, respectively. Therefore, the mode-locked laser is designed to operate in net anomalous

Optics EXPRESS

dispersion regime. Theoretically, a mode-locked laser is predictably stable if soliton operation takes place in the laser cavity. To generate soliton mode-locked laser, the dispersion and Kerr nonlinearity need to be delicately balanced [30]. Mode-locked laser that operates in anomalous dispersion provides negative chirping to balance the positive chirping of self-phase modulation phenomenon from Kerr nonlinearity effect imposed on the pulse propagation.

Figures 4(a) and 4(b) illustrates the optical spectra evolution of MLFL-U measured by an optical spectrum analyzer with bandwidth resolution of 0.02 nm from 1520 to 1550 nm and from 1540 to 1570 nm wavelength spans for λ(-) and λ(+) optical loops, respectively. The continuous wave and mode-locked lasers pump power threshold for λ(-) and λ(+) optical loops are measured at 21.0 and 22.6 mW, respectively. The 3-dB spectral bandwidth (Δλ) measurement for λ(-) and λ(+) optical loops are presented in Fig. 4(c) and 4(d), which exhibit an increase of Δλ as a function of pump power. At 222.7 mW maximum pump power, the obtained lasing central wavelength are 1533.40 and 1556.11 nm, and Δλ are measured at 2.75 and 3.14 nm for λ(-) and λ(+) optical loops, respectively. Our proposal presents wider Δλ than [18], which utilizes graphene SA to generate dual-lasing ML-EDFL. Wider Δλ produces shorter pulse duration for a transform-limited pulse. The presence of Kelly's sidebands indicates periodic perturbation between dispersion and nonlinearity in the laser cavity, which is the characteristic of soliton operation in fiber lasers. On the other hand, the absence of competing continuous wave components in the output spectrum indicates that the polarization state is properly controlled and the mode-locked EDFL operation is stable [31].

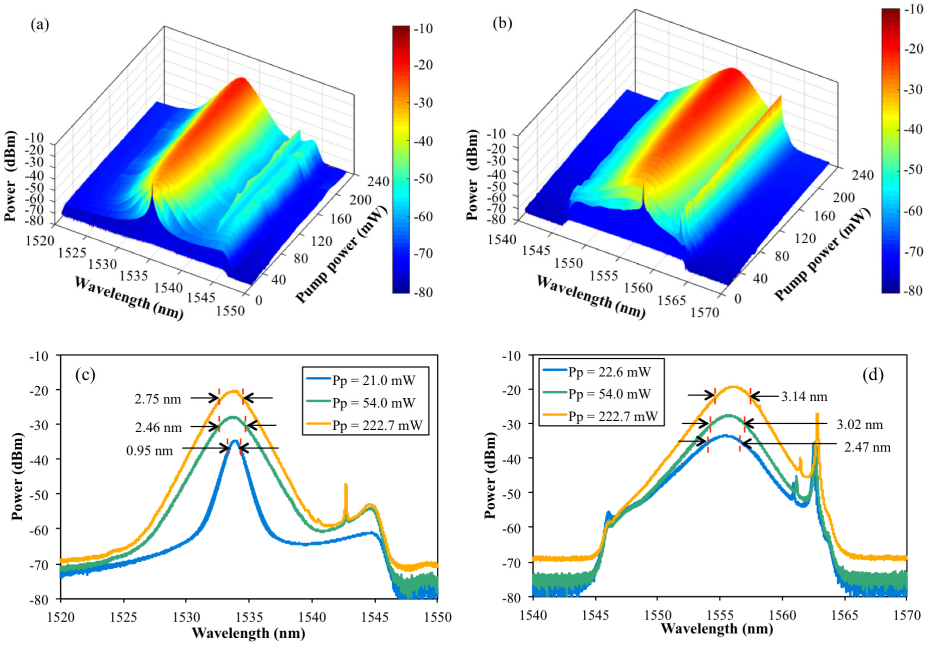

Fig. 4. Output spectrum of (a) λ(-) and (b) λ(+) optical loops with spectral bandwidth measurement in (c) and (d), respectively as a function of pump powers.

The FWHM pulse duration (τ_{FWHM}) of the MLFL-U is measured using an autocorrelator. The $sech^2$ fitted autocorrelation traces of MLFL-U are presented in Fig. 5, with τ_{FWHM} measurement at 900 and 940 fs for λ(-) and λ(+) optical loops, respectively. Overall, the pulse duration obtained in this work is comparatively shorter than the reported pulse duration in other works on multi-wavelength mode-locked EDFL [18].

Optics EXPRESS

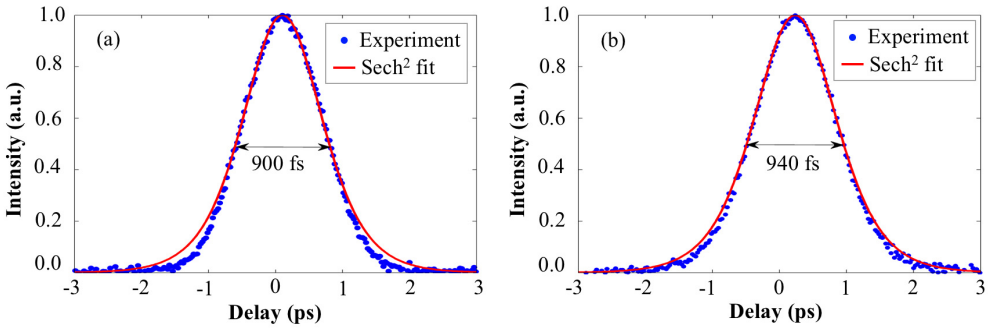

Fig. 5. Autocorrelation trace of (a) λ(-) and (b) λ(+) optical loops.

Another important parameter of a mode-locked pulse is the time bandwidth product (TBP), which is necessary for measuring the deviation of an executed pulse from the chirped-free Fourier transform-limited pulse. The TBP of a pulse can be defined as $\Delta\tau \times \Delta\nu \geq K$ where $\Delta\tau$ is the pulse duration at full-width at half-maximum, $\Delta\nu$ is the spectral bandwidth in frequency domain at FWHM and K is the lowest limitation value achievable for transform-limited pulse. The lowest limitation of K for sech^2 pulse profile is 0.315, assuming a chirp-free Fourier transform-limited pulse. The calculated TBP of the MLFL-U is recorded in Table 1. From this table, λ(-) optical loop is almost chirp-free. Contrarily, λ(+) optical loop is slightly chirped. Therefore, λ(+) optical loop with stronger chirping effect than λ(-) optical loop produces longer pulse duration despite the wider spectral bandwidth.

Table 1. TBP value for executed pulses from MLFL-U.

Optical loops	Δν (THz)	Δτ (ps)	TBP
λ (-)	0.3509	0.91	0.3192
λ (+)	0.3890	0.94	0.3657

The output pulse trains of the mode-locked lasers are measured using an oscilloscope and a photodetector. The oscilloscope traces of MLFL-U are depicted in Fig. 6. Based on experimental findings, single pulses are observed for both λ(-) and λ(+) optical loops. In this case, the background is clear without random and chaotic noise-like pulsing which could affect pulse stability [32]. The response time is measured at 119.1 and 109.9 ns, which corresponds to pulse repetition rate of 8.4 and 9.1 MHz for λ(-) and λ(+) optical loops, respectively. The measurements of pulse repetition are in good agreement with the cavity round-trip time.

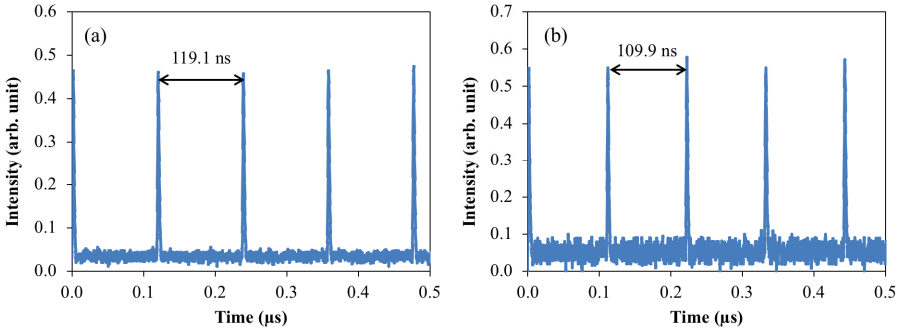

Fig. 6. Oscilloscope trace of (a) λ(-) and (b) λ(+) optical loops.

The frequency spectrum of the mode-locked lasers is measured using an electrical spectrum analyzer. In this measurement, the frequency domain is set at a span of 50 MHz with a bandwidth resolution of 300 Hz. Figure 7 presents the frequency spectra of the MLFL-

Optics EXPRESS

U optical pulses at fundamental frequencies. The peak to pedestal extinction ratio (PER) is measured according to the first order frequency-domain pulse of the MLFL-U. The highest PER measurement of the MLFL-U outputs are 63.1 and 61.8 dB for λ(-) and λ(+) optical loops, respectively at 22.6 mW pump power. From these findings, PER more than 60 dB indicates a stable mode-locked laser pulse as denoted in [33].

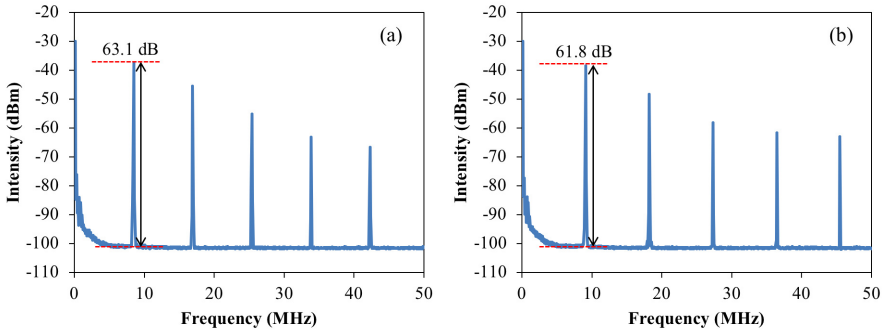

Fig. 7. Frequency spectrum of (a) λ(-) and (b) λ(+) optical loops.

The output power and pulse energy development from the λ(-) and λ(+) optical loops of the MLFL-U is illustrated in Fig. 8(a) and 8(b), respectively. Four regions are denoted; Region A represents spontaneous emission region, Region B is denoted as continuous wave laser, Region C is identified as single pulsed mode-locked laser, and Region D denotes multiple pulses mode-locked laser region. After the mode-locked laser threshold is exceeded, average output power evolves from 0.23 to 11.63 mW and pulse energy increases from 0.027 to 1.38 nJ for λ(-) optical loop as portrayed in Fig. 8(a). Based on Fig. 8(b), the average output power develops from 0.25 to 14.27 mW, corresponding to the evolution of pulse energy from 0.027 to 1.57 nJ for λ(+) optical loop.

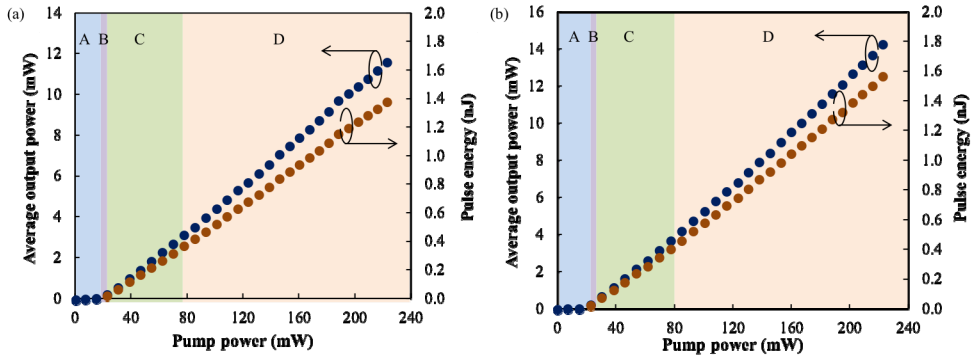

Fig. 8. Output power and pulse energy development for the (a) λ(-) and (b) λ(+) optical loops of MLFL-U.

Figure 9 depicts the stability test of MLFL-U at 222.7 mW maximum pump power over an observation time of 60 minute. This measurement is recorded every two-minute time interval. Based on the observation in Fig. 9(a) and 9(b), the MLFL-U is well maintained for both λ(-) and λ(+) optical loops without significant disruption to the lasing wavelength or mode-locked laser operation. In addition, Fig. 9(c) shows the power stability of the dual-wavelength mode-locked lasers. The λ(-) and λ(+) optical loops show corresponding maximum variation within 0.10 dB and 0.07 dB over 60 minute observation period. Therefore, this proposed MLFL-U yields a practical seed laser source to be employed in pulsed laser system device due to its high laser stability.

Optics EXPRESS

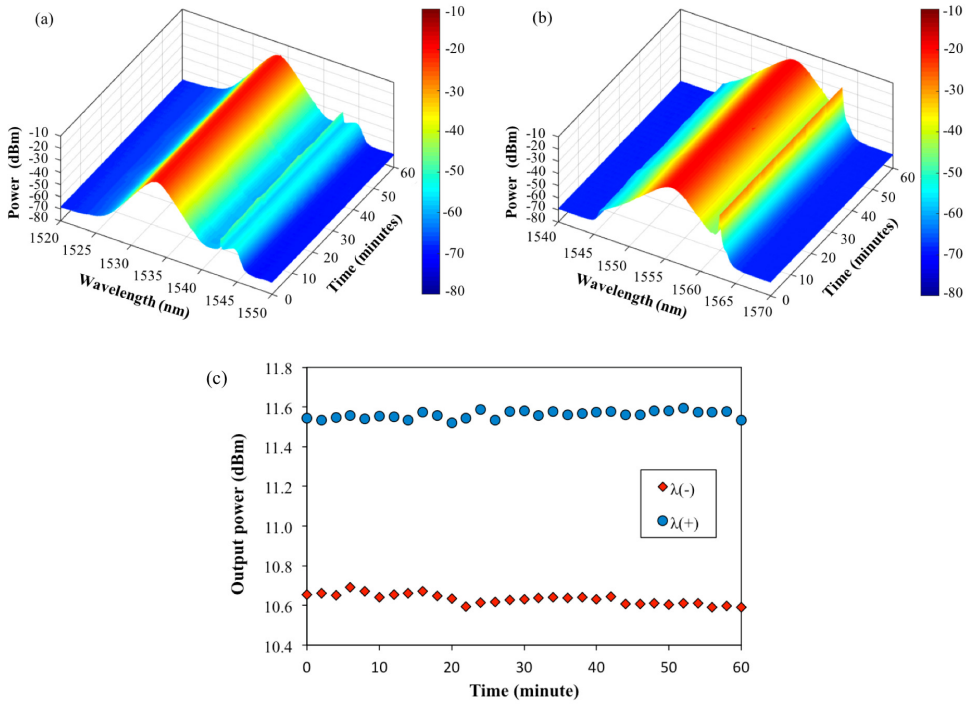

Fig. 9. Stability test of (a) λ(-) and (b) λ(+) optical loops of MLFL-U, (c) power stability over an observation time of 60 minute.

The summary of this research compared to previous related works with graphene is presented in Table 2. By utilizing similar SA structure and material composition to the work in [17], this research work establishes shorter τ_{FWHM} with closely spaced dual-wavelength mode-locked lasers within C-band region. Moreover, this work also shows improvement over D-shaped monolayer graphene-SA through wider Δλ and shorter τ_{FWHM} [18].

Table 2. Summary of research comparison to previous works.

SA structure	λ_c (nm)	Δλ (nm)	τ_{FWHM} (ps)	Ref.
Graphene/PMMA sandwiched	1558.5	3.9	0.92	[17]
between two fiber ferrules	1938.0	2.6	1.57	
Monolayer graphene film covered on	1531.5	1.9	1.39	[18]
D-shaped fiber	1559.1	2.1	1.60	
Graphene/PMMA sandwiched	1533.4	2.8	0.90	This
between two fiber ferrules	1556.1	3.1	0.94	work

5. Conclusion

In this work, a GPSA is fabricated and its functionality is validated by mode-locking dual-wavelength EDFLs. The fabrication of GPSA is achieved by transferring commercially available GPTF onto a fiber ferrule. This simple process produces GPSA with modulation depth of 6%. The fiber laser configuration utilizes unidirectional laser signal oscillation through a common gain medium and GPSA. The proposed dual-wavelength mode-locked EDFLs successfully generate $sech^2$-fitted pulse duration of 900 and 940 fs at approximately 1530 and 1560 nm wavelengths, respectively. The fundamental pulses occur simultaneously at low mode-locked threshold of 22.6 mW with closely spaced dual wavelength femtosecond lasers in 1.53 and 1.56 μm wavelength regions. In addition, this work highlights the feasibility of doubling the number of femtosecond pulsed laser outputs with minimal usage of optical components including saturable absorbers.

Optics EXPRESS

Funding

Ministry of Higher Education, Malaysia (GP-IPB/2014/9440700); Royal Society-Newton-Ungku Omar Advanced Fellowship (NA150463).